# Inorganic Chemistry

Article

# Forum

## Electronic Design Criteria for O–O Bond Formation via Metal–Oxo Complexes

**Theodore A. Betley,**[†] **Qin Wu,**[‡] **Troy Van Voorhis,**[‡] **and Daniel G. Nocera**[*,‡]

*Department of Chemistry, Massachusetts Institute of Technology, 77 Massachusetts Avenue, 6-335, Cambridge, Massachusetts 02139-4307, and Department of Chemistry and Chemical Biology, Harvard University, 12 Oxford Street, Cambridge, Massachusetts 02138*

Metal–oxos are critical intermediates for the management of oxygen and its activation. The reactivity of the metal–oxo is central to the formation of O–O bonds, which is the essential step for oxygen generation. Two basic strategies for the formation of O–O bonds at metal–oxo active sites are presented. The acid–base (AB) strategy involves the attack of a nucleophilic oxygen species (e.g., hydroxide) on an electrophilic metal–oxo. Here, active-site designs must incorporate the assembly of a hydroxide (or water) proximate to a high-valent metal–oxo of even d electron count. For the radical coupling (RC) strategy, two high-valent metal–oxos of an odd d electron count are needed to drive O–O coupling. This Forum Article focuses on the different electronic structures of terminal metal–oxos that support AB and RC strategies and the design of ligand scaffolds that engender these electronic structures.

## 1. Introduction

The interaction of an O atom with a metal center was described in this journal by the molecular orbital (MO) diagram of Figure 1 nearly 50 years ago.[1] At the most rudimentary level, this model for the interaction of an O atom with a metal has not changed. Metal d orbitals interact with the 2p valence orbitals of oxygen to engender the energy level ordering shown in Figure 1. The diagram can be obtained by replacing the axial ligand of a $ML_6$ octahedral complex with oxygen. This substitution lowers the $t_{2g}$ orbital symmetry to $b_2(d_{xy})$ and $e(d_{xz},d_{yz})$ and the metal–ligand $\sigma$-antibonding $e_g$ orbital symmetry to $b_1(d_{x^2-y^2})$ and $a_1(d_{z^2})$ levels. Because the metal–oxo bond is short, the $d_{z^2}$ orbital is more destabilized than in its $ML_6$ parent. Similarly, the $e(d_{xz},d_{yz})$ orbitals are destabilized relative to their octahedral parentage because they are $\pi$-antibonding with respect to the O $2p_x$ and $2p_y$ orbitals (orbital interaction shown in Figure 1). Owing to the prevalence of these $\sigma$ and $\pi$ interactions of

the oxo with the metal, the axial ligand opposite to the oxo is significantly weakened or typically absent.

With an electronic structure established, the stability (and reactivity) of the oxo is largely determined by the d electron count. For $d^2$ systems such as $Mn^V$, the electrons often are paired, residing in the $d_{xy}$ orbital. The $e(d_{xz},d_{yz})$ orbital set is empty and able to accept the $p_x$ and $p_y$ electron pairs from oxo to effectively form a Mn–O triple bond. If two electrons reside in $e(d_{xz},d_{yz})$, such as the case for $Fe^{IV}$, then a double bond is obtained. The electron pair in the $d_{xy}$ orbital, as far as the oxo is concerned, is a spectator, but the pair, nevertheless, does have an effect. If the electrons are removed completely from $d_{xy}$, i.e., a $d^0$ metal center such as $M = V^V$, $Ti^{IV}$, or $Zr^{IV}$, the M–O bond becomes exorbitantly stable and the oxo is extremely difficult to activate. Conversely, for late transition metals of reasonable oxidation states (less than $M^{4+}$) such as Co, Cu, and Ni, the $e(d_{xz},d_{yz})$ orbital sets are filled. The oxo thus cannot donate its $p\pi$ electron pairs to the metal and a multiple metal–oxo bond cannot be supported.
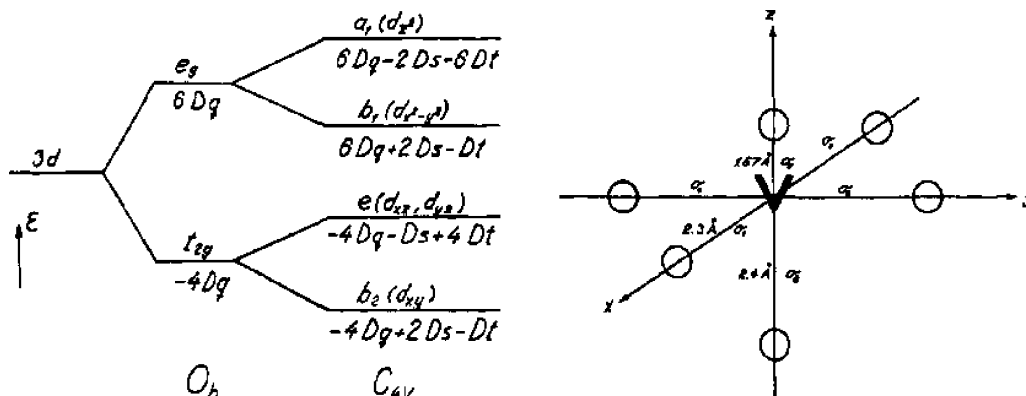
It should therefore come as no surprise that Nature found the middle ground of the periodic table to manage multiply bonded oxos with special emphasis on iron and manganese.

---

\* To whom correpondence should be addressed. E-mail: nocera@mit.edu.
† Harvard University.
‡ Massachusetts Institute of Technology.
(1) Ballhausen, C. J.; Gray, H. B. *Inorg. Chem.* **1962**, *1*, 111–122.

**Figure 1.** Original d-orbital splitting diagram for the metal−oxo interaction (of the vanadyl ion). Reproduced with permission from ref 1. Copyright 1962 American Chemical Society.

In the heme iron centers of monooxygenases,[2–5] the metal−oxo is generated within the tetragonal field of the porphyrin macrocycle. The diversity of biological redox processes performed by these enzymes is achieved by a $d^4$ metal−oxo, compound I (Cpd I),[2–4,6,7] which is two redox levels above $Fe^{III}$ with a ferryl $Fe^{IV}$=O and associated radical (e.g., a porphyrin $\pi$-radical cation, $P^{\bullet+}$, in horseradish peroxidase and catalase or an oxidized tryptophan in cytochrome $c$ peroxidase [CcP]). Of pertinence to this Forum issue, metal−oxos prevail in the oxygen-making chemistry of the photosynthetic membrane. The appearance of the structures of the photosynthetic membrane suggests various possibilities, shown in Figure 2, for oxygen generation from the S4 Kok state[8] of the oxygen-evolving complex (OEC).[9–12] In all cases, oxygen generation is proposed to arise from oxos associated with a highly oxidized {Mn₄Ca} cluster. In one formalism, a $d^2$ metal−oxo is posited as the intermediate in oxygen generation. If all of the oxidizing equivalents are borne by the manganese centers, a {$Mn^{IV}_3Mn^V$} core is obtained. In this case, an electrophilic oxo at the "dangler" $Mn^V$ center[13] of OEC is proposed to be attacked by a nucleophilic hydroxide to form the O−O bond.[14] Alternatively, radical character has also been pro-
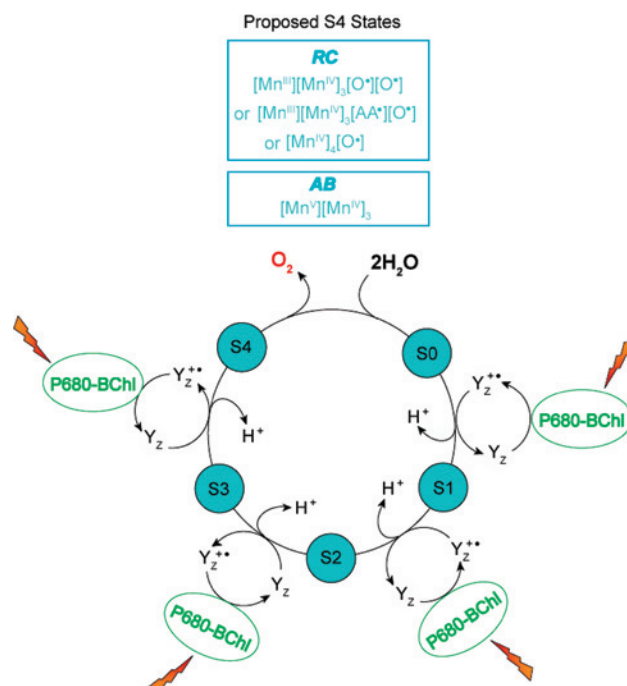


**Figure 2.** Proposed intermediates for the OEC cluster in the $S_4$ state of the Kok cycle and the O−O bond-forming strategy to which they correlate. The various proposals of the $S_4$ state were put forth at the Royal Society Discussion *Revealing How Nature Uses Sunlight To Split Water*, held in London in April 2007.
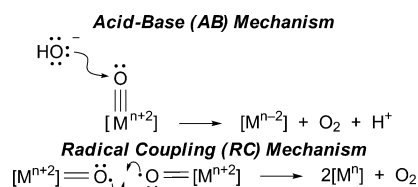
posed to reside on two oxos of a {$Mn^{III}Mn^{IV}_3,O^{\bullet},O^{\bullet}$} cofactor or one in which one of the radical centers resides on an amino acid, {$Mn^{III}Mn^{IV}_3,O^{\bullet},AA^{\bullet}$} (AA = amino acid). In this case, one may envisage O−O bond formation to occur by coupling of the biradical pair; this model gives credence to proposals of oxygen generation via peroxide-like intermediates.[15,16] A {$Mn^{IV}_4,O^{\bullet}$} core places a single radical spin on the O atom and oxygen is generated by an undefined strategy.

This Forum Article will focus on electronic structures of metal−oxos that can support the O−O bond. New ligands that engender these variegated electronic structures and the O−O bond formation strategies derived from these different ligand fields will be presented.

(2) Sono, M.; Roach, M. P.; Coulter, E. D.; Dawson, J. H. *Chem. Rev.* **1996**, *96*, 2841–2887.
(3) Dunford, H. B. *Heme Peroxidases*; Wiley: New York, 1999.
(4) Watanabe, Y. In *The Porphyrin Handbook*; Kadish, K. M., Smith K. M., Guilard, R., Eds.; Academic Press: San Diego, 2000; Vol. *4*, pp 97–117..
(5) Meunier, B.; de Visser, S. P.; Shaik, S. *Chem. Rev.* **2004**, *104*, 3947–3980.
(6) *Cytochrome P-450 Structure, Strategy and Biochemistry*, 2nd ed.; Ortiz de Montellano, P. R., Ed.; Plenum Press: New York, 1995.
(7) Newcomb, M.; Zhang, R.; Chandrasena, R. E. P.; Halgrimson, J. A.; Horner, J. H.; Makris, T. M.; Sligar, S. G. *J. Am. Chem. Soc.* **2006**, *128*, 4580–4581.
(8) Haumann, M.; Liebisch, P.; Muller, C.; Barra, M.; Grabolle, M.; Dau, H. *Science* **2005**, *310*, 1019–1021.
(9) Ferreira, K. N.; Iverson, T. M.; Maghlaoui, K.; Barber, J.; Iwata, S. *Science* **2004**, *303*, 1831–1838.
(10) Iwata, S.; Barber, J. *Curr. Opin. Struct. Biol.* **2004**, *14*, 447–453.
(11) Yano, J.; Kern, J.; Sauer, K.; Latimer, M. J.; Pushkar, Y.; Biesiadka, J.; Loll, B.; Saenger, W.; Messinger, J.; Zouni, A.; Yachandra, V. *Science* **2006**, *314*, 821–825.
(12) Loll, B.; Kern, J.; Saenger, W.; Zouni, A.; Biesiadka, J. *Nature* **2005**, *438*, 1040–1044.
(13) Peloquin, J. M.; Campbell, K. A.; Randall, D. W.; Evanchik, M. A.; Pecoraro, V. L.; Armstrong, W. H.; Britt, R. D. *J. Am. Chem. Soc.* **2000**, *122*, 10926–10942.

(14) McEvoy, J. P.; Brudvig, G. W. *Chem. Rev.* **2006**, *106*, 4455–4483.
(15) Ruttinger, W.; Dismukes, G. C. *Chem. Rev.* **1997**, *97*, 1–24.
(16) Siegbahn, P. E. M. *Chem.—Eur. J.* **2006**, *12*, 9217–9227.

**Chart 1**



***Acid-Base (AB) Mechanism***

$$[M^{n+2}] \longrightarrow [M^{n-2}] + O_2 + H^+$$

***Radical Coupling (RC) Mechanism***

$$[M^{n+2}]=\ddot{O}. \quad .\ddot{O}=[M^{n+2}] \longrightarrow 2[M^n] + O_2$$

## 2. Mechanistic Possibilities for Conversion of Oxygen from Metal−Oxos

Metal−oxos appear as critical intermediates in the management of oxygen and its activation. The reactivity of the metal−oxo is largely determined by the ligand field of the metal and its d electron count. Metals with high d electron counts generally cannot support an oxo. For very low electron counts, the metal−oxo bond tends to be too stable for activation. We wish to develop an unusual ligand field for the metal−oxo, one that supports metals with high d electron counts and promotes reactivity of the oxo.

Chart 1 presents two proposed strategies for initiating O−O bond formation utilizing metal−oxo complexes. Both strategies require the intermediacy of a metal−oxo derived from water, where the oxo reactivity is dictated by the metal's local geometry and electron configuration.

### 2.1. Nucleophilic Attack of Hydroxide on High-Valent Metal−Oxo.
Chart 1 (acid−base, AB, strategy) depicts oxygen acting as both a nucleophile and an electrophile. In this AB strategy, an oxygen nucleophile (e.g., water or hydroxide) attacks a metal-bound, electrophilic oxo. The metal oxidation state and geometry play key roles in contributing to the electrophilicity of the oxo ligand. From an orbital perspective, an orbital of $\sigma$ character (highest occupied molecular orbital) approaches the M−O $\pi^*$ orbital (lowest unoccupied molecular orbital). The combination leads to the formation of an O−O $\sigma$ bond while breaking one of the M−O $\pi$ bonds, representing a formal $2e^-$ reduction of the metal center. The AB strategy describes the O−O bond-forming chemistry of the $\{Mn^{IV}_3Mn^V\}$ model for the $S_4$ state in Figure 2. Stepwise oxidation with concomitant proton extrusion from a water-ligated manganese center results in the formation of a manganyl−oxo complex. The oxygen from the calcium-bound water/hydroxide nucleophilically adds to the oxo, forming the O−O bond. It should be noted that the AB strategy can be considered the microscopic reverse of the O−O bond heterolysis step in cytochrome P450 to produce water and a ferryl.[17,18] In this regard, the oxo of the $d^4$ iron center of heme monooxygenases is related to the oxo of the $d^2$ manganese center of OEC. The remarkable chemical, mechanistic, and structural similarities of the oxygen bond-forming chemistry at the manganese−oxo center of the OEC active site in photosystem II to that of the oxygen bond-breaking chemistry at the iron−oxo active sites of heme monooxygenases have been previously noted.[19,20]

### 2.2. Radical Coupling of Two Metal−Oxos.
An alternative mechanistic possibility for O−O bond formation involves the coupling of two oxygen-based radicals (RC strategy, Chart 1). For high-valent metal−oxo species bearing radical character, the coupling strategy involves O−O bond formation between two orbitals of M−O $\pi^*$ parentage as the singly occupied molecular orbital. We note that direct coupling of the radicals is not necessary and may very well be mediated by water. Indeed, our most recent computations suggest that a direct coupling strategy is energetically unfavorable and likely involves the participation of water (see section 4.1). While this strategy has no definitive biological precedent, in our opinion, the RC strategy is the simplest strategy that describes the electrochemical conversion of water to oxygen by ruthenium polypyridyl complexes in high oxidation states (see section 4.1).[21−23]

## 3. MO Description of Different Ligand Fields for Metal−Oxos

The MO splitting diagram depicted in Figure 3A correlates directly to the initial electronic description of a metal−oxo in a tetragonal field (Figure 1). The latter is furnished by replacement of an axial ligand of an octahedron with a terminal oxo ligand. This substitution destabilizes both the $d_{z^2}$ and degenerate $d_{xz}$ and $d_{yz}$ orbitals to form M−O $\sigma$ and two $\pi$ bonds in the tetragonal ligand field. In a local $C_4$ environment, preservation of the oxo moiety is typically found in metals with a d electron count of 4 or less. The first two electrons can populate an essentially nonbonding $d_{xy}$ orbital, but the subsequent addition of electrons populates the degenerate M−O $\pi^*$ orbitals (approximately $d_{xz}$ and $d_{yz}$). Exemplary of this electronic structure, the M−O bond distance of $[(HMPA-B)Mn^V(O)]^-$ [HMPA-B; 1,2-bis(2-hydroxy-2-methylpropanamido)benzene][24] is consistent with that expected for a triple bond, whereas the M−O bond distance of the ground-state triplet ($S = 1$) $[(TMC)Fe^{IV}(O)]^{2+}$ [TMC; 1,4,8,11-tetraazacyclotetradecane] is in accordance with a double bond.[25]

Changing the geometry about the metal−oxo to a local $C_3$ trigonal ligand field presents a different criterion for stabilization of a terminal metal−oxo bond. For a trigonal-bipyramidal ligand field (Figure 3B), the two lowest-lying orbitals comprise the M−O $\pi^*$ interactions. Hence, a metal−oxo triple bond may be preserved only for a $d^0$ metal center. A metal−oxo double bond, which is expected to be unstable owing to the strong trans-directing influence of the

(17) Shaik, S.; Kumar, D.; De Visser, S. P.; Altun, A.; Thiel, W. *Chem. Rev.* **2005**, *105*, 2279–2328.

(18) Denisov, I. G.; Makris, T. M.; Sligar, S. G.; Schlichting, I. *Chem. Rev.* **2005**, *105*, 2253–2277.

(19) Hoganson, C. W.; Pressler, M. A.; Proshlyakov, D. A.; Babcock, G. T. *Biochim. Biophys. Acta* **1998**, *1365*, 170–174.

(20) Chang, C. J.; Chang, M. C. Y.; Damrauer, N. H.; Nocera, D. G. *Biophys. Biochim. Acta* **2004**, *1655*, 13–28.

(21) Gersten, S. W.; Samuels, G. J.; Meyer, T. J. *J. Am. Chem. Soc.* **1982**, *104*, 4029–4030.

(22) Sens, C.; Romero, I.; Rodriguez, M.; Llobet, A.; Parella, T.; Benet-Buchholz, J. *J. Am. Chem. Soc.* **2004**, *126*, 7798–7799.

(23) Zong, R.; Thummel, R. P. *J. Am. Chem. Soc.* **2005**, *127*, 12802–12803.

(24) Collins, T. J.; Gordon-Wylie, S. W. *J. Am. Chem. Soc.* **1989**, *111*, 4511–4513.

(25) Rohde, J.-U.; In, J.-J.; Lim, M. H.; Brennessel, W. W.; Bukowski, M. R.; Stubna, A.; Münck, E.; Nam, W.; Que, L., Jr *Science* **2003**, *299*, 1037–1039.
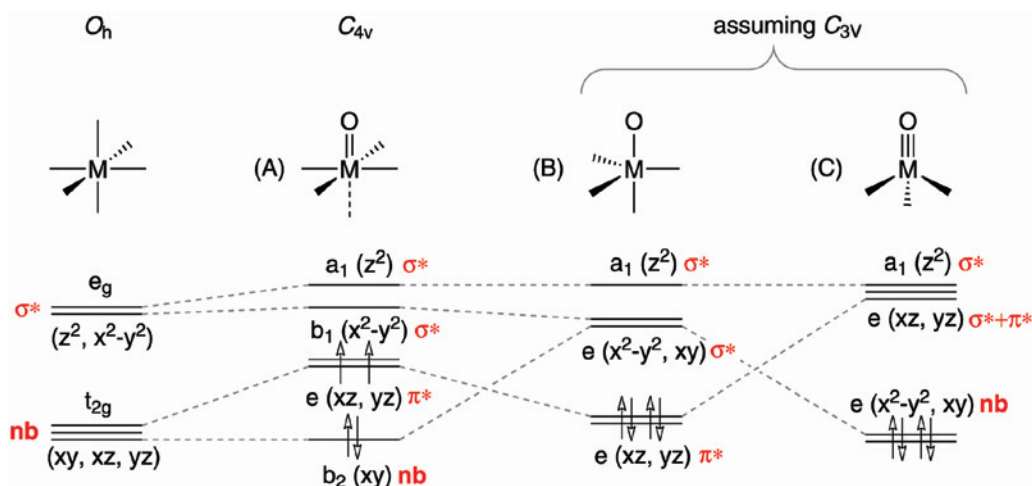
**Figure 3.** Qualitative frontier MO splitting diagrams for a metal−oxo residing in a (A) tetragonal ligand field, (B) trigonal-bipyramidal ligand field, and (C) tetrahedral ligand field. The d electron count and respective bond order is shown for possible configurations for a $d^4$ electron count.

apical ligand, if present at all, can be maintained only for a $d^2$ center. However, an interesting electronic structure is obtained when the apical ligand opposite to the metal−oxo vector is removed, as shown in Figure 3C. The metal-based orbitals involved in the $\sigma$ and $\pi$ M−O interactions are the highest in energy owing to their antibonding character. The precise ordering of the $a_1(d_{z^2}(\sigma^*))$ and $e(d_{xz},d_{yz}(\pi^*))$ depends on the tridentate ligand's bite angle.[26] This ordering notwithstanding, the distinguishing trait of this ligand field for the metal−oxo is that a degenerate $e(d_{x^2-y^2},d_{xy})$ level is lowest in energy and may accommodate up to four d electrons ($S = 0$) without destabilizing the oxo $\sigma$ or $\pi$ bonding frameworks. Thus, targeting this framework allows for the design of triple (and double) bonded metal−oxos with middle-to-late transition metals.

## 4. Metal−Oxos in Tetragonal Fields

**4.1. Pseudooctahedral Metal−Oxo Complexes.** Whereas octahedral, triply bonded, terminal oxo complexes to the right of the manganese triad on the periodic table are very rare,[27,28] there are many terminal oxo complexes with a bond order of less than 3 in the iron triad. Populating the M−O $\pi^*$ orbitals with one or two electrons can serve to stabilize the oxo linkage ($d^4$, BO$_{M-O}$ = 2) or create a potent odd-electron oxidant ($d^3$, BO$_{M-O}$ = 2.5) that localizes a radical within the M−O $\pi^*$ MO. This $d^3$ oxo "radical" electronic structure in a pseudooctahedral field describes the electronic structure of $[(bpy)_2(OH_2)Ru^{III}(\mu-O)Ru^{III}(OH_2)(bpy)_2]^{4+}$ (**1**, Chart 2), which is the parent molecule of the only authentic class of homogeneous water-splitting catalysts.[21]

Meyer's blue dimer complex,[21] $[(bpy)_2(OH_2)Ru^{III}(\mu-O)Ru^{III}(OH_2)(bpy)_2]^{4+}$, and related analogues[22,23] catalyze the oxidation of water at modest overpotentials and turnovers. Such species are composed of a dimeric ruthenium core

**Chart 2**
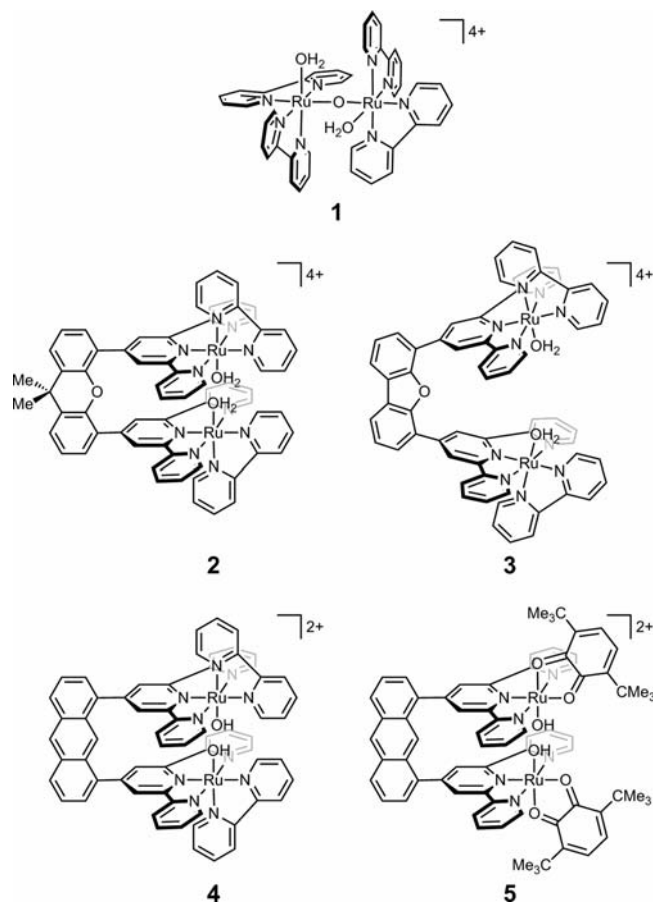


connected by a nearly linear $\mu$-oxo bridge. Ancillary bipyridyl ligands complete the coordination sphere of each metal. Global kinetic analysis of UV–vis spectral changes accompanying the oxidation of the blue dimer reveals that the initial $[(OH_2)Ru^{III}(\mu-O)Ru^{III}(OH_2)]$ core undergoes a series

(26) Jenkins, D. M.; Di Bilio, A. J.; Allen, M. J.; Betley, T. A.; Peters, J. C. *J. Am. Chem. Soc.* **2002**, *124*, 15336–15350.

(27) Anderson, T. M.; Neiwert, W. A.; Kirk, M. L.; Piccoli, P. M. B.; Schultz, A. J.; Koetzle, T. F.; Musaev, D. G.; Morokuma, K.; Cao, R.; Hill, C. L. *Science* **2004**, *306*, 2074–2077.

(28) Anderson, T. M.; Cao, R.; Slonkina, E.; Hedman, B.; Hodgson, K. O.; Hardcastle, K. I.; Neiwert, W. A.; Wu, S.; Kirk, M. L.; Knottenbelt, S.; Depperman, E. C.; Keita, B.; Nadjo, L.; Musaev, D. G.; Morokuma, K.; Hill, C. L. *J. Am. Chem. Soc.* **2005**, *127*, 11948–11949.

of coupled proton and electron transfers to produce a $[(O)Ru^V(\mu\text{-}O)Ru^V(O)]$ species that precedes the O–O bond.[29] In the course of oxidation, an intermediate $Ru^{IV}Ru^{IV}$ species is not observed owing to its instability to disproportionation to yield $Ru^{III}Ru^{IV}$ and $Ru^VRu^{IV}$ species, which are believed to be oxidized by one electron to the $Ru^VRu^V$ dimer. The odd-electron system may be formulated as side-by-side pseudooctahedral oxo radical centers, though their direct coupling has not been implicated as a dominant reaction pathway. If such a RC strategy is important, then the structural and electronic features unique to the blue dimer inhibit the most straightforward reaction path: a direct coupling. Geometric constraints imposed by the ancillary ligands and the $\mu$-oxo bridge prevent O atoms from attaining the correct geometry to form an O–O bond. It has been estimated that rotation about the $\mu$-oxo bond to yield an eclipsed geometry of the M–O vectors still places the O atoms 3.2 Å apart.[30] Coupling at this distance would require a significant structural distortion. In addition, computational studies suggest that there exists weak antiferromagnetic coupling between the ruthenium centers.[31] Putative radical character will be diminished by antiferromagnetic coupling through the $\mu$-oxo bridge.[32]

In light of these barriers to implementing a direct RC strategy in a side-by-side $Ru^VRu^V$ dioxo pseudooctahedron, we and others[48,49] have designed systems that remove these impediments while largely retaining the other features of the blue dimer system. We have pursued a "Pacman" ligand design wherein dimethylxanthene and dibenzofuran organic spacers are used as scaffolds to preorganize metal centers in a cofacial arrangement.[33–36] In the Pacman approach,[37,38] metal centers are electronically isolated from each other by imposing the long covalent pathway between them via the scaffold, but they are flexible enough to accommodate over a 4 Å range in the metal–metal distance.[39–41] Such flexibility is advantageous inasmuch as the metal center may clamp down on small molecules to facilitate their activation within the cleft and then spring open to release the substrate.[42–45] Adaptation of the Pacman approach to the $Ru^V$–O permits
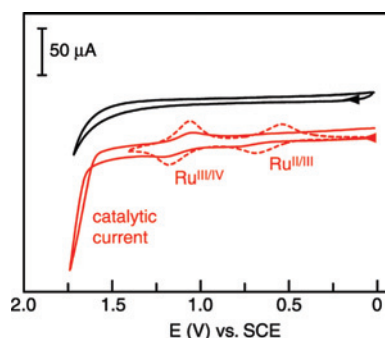


**Figure 4.** Cyclic voltamograms recorded using a glassy carbon electrode coated with no catalyst (black) and the DTX catalyst **2** (red) referenced to Ag/AgCl.

the Ru–O vectors to be oriented in a collinear fashion for their direct coupling as opposed to the gauche disposition found in Meyer's original system.

The DPX- and DPD-bridged ruthenium(II) terpyridyl complexes **2** and **3**, shown in Chart 2, have been prepared with bypyridine ligands completing the primary coordination sphere of each ruthenium center. Preliminary electrochemical studies indicate that the Pacman complexes are stable through the range of oxidation states of $Ru^{II}$ to $Ru^{IV}(O)$. As shown in Figure 4 for **3**, two discrete two-electron oxidations are observed (0.1 M KPF$_6$, pH = 6.8) to generate [(DTX)-((bpy)$Ru^{IV}$=O)$_2$]$^{4+}$. The two-electron waves (one electron from each metal) show no evidence of splitting, indicating that the ruthenium centers are not in electronic communication. Further oxidation of the [$Ru^{IV}(O)$]$_2$ Pacman complex is characterized by an irreversible and pronounced catalytic current. Oxygen production accompanies oxidation, as has been verified by a standard pyrogallol analysis. The monomeric $Ru^V$ congeners of **2** and **3** are inert toward water oxidation to oxygen,[46,47] suggesting that both metal centers are involved, even if the strategy is not direct RC. The precise nature of the RC mechanism for **3** has been probed computationally using density functional theory for the $\{[Ru^{IV}(O)]_2\}^{4+}$ precatalytic state. At equilibrium, the metal–oxo groups are held together by a water bridge that results in a relatively long O–O separation of 7.4 Å. Forcing the two oxo groups closer to one another yields the energy profile in Figure 5. As the two [$Ru^{IV}(O)$]$^{2+}$ groups approach each other, the energy rises steadily primarily because of an increase in electrostatic repulsion, with smaller effects due to steric crowding at the active site and bond angle strain on the scaffold. As a result, a barrier of 55 kcal/mol must be overcome if the two oxos are to become close enough to

(29) Binstead, R. A.; Chronister, C. W.; Ni, J.; Hartshorn, C. M.; Meyer, T. J. *J. Am. Chem. Soc.* **2000**, *122*, 8464–8473.

(30) Gilbert, J. A.; Eggleston, D. S.; Murphy, W. R., Jr.; Geselowitz, D. A.; Gersten, S. W.; Hodgson, D. J.; Meyer, T. J. *J. Am. Chem. Soc.* **1985**, *107*, 3855–3864.

(31) Yang, X.; Baik, M.-H. *J. Am. Chem. Soc.* **2004**, *126*, 13222–13223.

(32) Yang, X.; Baik, M.-H. *J. Am. Chem. Soc.* **2006**, *128*, 7476–7485.

(33) Chang, C. J.; Deng, Y.; Heyduk, A. F.; Chang, C. K.; Nocera, D. G. *Inorg. Chem.* **2000**, *39*, 959–966.

(34) Chang, C. J.; Deng, Y.; Shi, C.; Chang, C. K.; Anson, F. C.; Nocera, D. G. *Chem. Commun.* **2000**, 1355–1356.

(35) Chang, C. J.; Yeh, C.-Y.; Nocera, D. G. *J. Org. Chem.* **2002**, *67*, 1403–1406.

(36) Chng, L. L.; Chang, C. J.; Nocera, D. G. *J. Org. Chem.* **2003**, *68*, 4075–4078.

(37) Rosenthal, J.; Nocera, D. G. *Acc. Chem. Res.* **2007**, *40*, 543–553.

(38) Rosenthal, J.; Nocera, D. G. *Prog. Inorg. Chem.* **2007**, *55*, 483–544.

(39) Deng, Y.; Chang, C. J.; Nocera, D. G. *J. Am. Chem. Soc.* **2000**, *122*, 410–411.

(40) Chang, C. J.; Baker, E. A.; Pistorio, B. J.; Deng, Y.; Loh, Z.-H.; Miller, S. E.; Carpenter, S. D.; Nocera, D. G. *Inorg. Chem.* **2002**, *41*, 3102–3109.

(41) Chang, C. J.; Deng, Y.; Peng, S.-M.; Lee, G.-H.; Yeh, C.-Y.; Nocera, D. G. *Inorg. Chem.* **2002**, *41*, 3008–3016.

(42) Pistorio, B. J.; Chang, C. J.; Nocera, D. G. *J. Am. Chem. Soc.* **2002**, *124*, 7884–7885.

(43) Hodgkiss, J. M.; Chang, C. J.; Pistorio, B. J.; Nocera, D. G. *Inorg. Chem.* **2003**, *42*, 8270–8277.
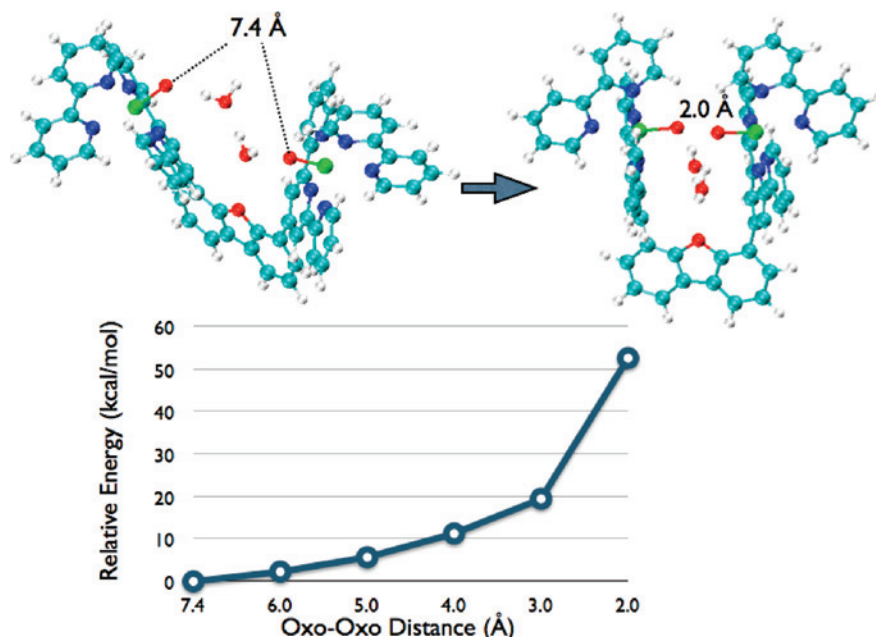
(44) Chang, C. J.; Loh, Z.-H.; Shi, C.; Anson, F. C.; Nocera, D. G. *J. Am. Chem. Soc.* **2004**, *126*, 10013–10020.

(45) Rosenthal, J.; Pistorio, B. J.; Chng, L. L.; Nocera, D. G. *J. Org. Chem.* **2005**, *70*, 1885–1888.

(46) McHatton, R. C.; Anson, F. C. *Inorg. Chem.* **1984**, *23*, 3935–3942.

(47) Takeuchi, K. J.; Thompson, M. S.; Pipes, D. W.; Meyer, T. J. *Inorg. Chem.* **1984**, *23*, 1845–1851.

(48) Wada, T.; Tsuge, K.; Tanaka, K. *Angew. Chem., Int. Ed.* **2001**, *39*, 1479–1482.

**Figure 5.** Computed energy profile for the direct coupling of oxo groups in the DPD-bridged $[Ru^{IV}(O)]_2^{4+}$ complex **3**. A combination of electrostatic and steric factors presents an extremely high barrier to direct association of the terminal oxo groups.

one another (2 Å) for their direct coupling. Further oxidation of this compound to $[Ru_2^{IV,V}(O)_2]^{5+}$ or $[Ru_2^{V,V}(O)_2]^{6+}$ will only increase this electrostatic barrier, indicating that O—O bond formation by direct coupling of oxo—base radicals of **3** is unlikely. Hence, if an RC strategy prevails, water appears to be needed to mediate that coupling.

Our results for the DTX and DTD Pacman complexes complement the results obtained for analogous Pacman complexes **4** and **5**.[48,49] Terpyridines appended to the anthracene spacer ligate two ruthenium centers whose coordination sphere is completed by a hydroxo ligand and either a bipyridine (**4**) or 3,6-di-*tert*-butyl-1,2-benzoquinone (**5**) ligand (Chart 2). Complex **4** affixed to an indium—tin oxide electrode exhibits a catalytic current at potentials greater than 1.7 V vs NHE. However, controlled-potential electrolysis at 1.90 V produced insufficient oxygen to be detected by gas chromatography. Conversely, the introduction of the redox-active benzoquinone ligand in **5** leads to a pronounced increase in oxygen production. Studies aimed at understanding the reasons for this enhanced activity of ruthenium Pacman systems possessing the redox-active 3,6-di-*tert*-butyl-1,2-benzoquinone ligands are currently underway.[50]

**4.2. Square-Pyramidal Metal—Oxo Complexes.** A $d^2$ electron count favors the stabilization of the M—O triple bond but not in an octahedral geometry. The strong trans influence of the oxo ligand dictates that a square-pyramidal geometry be adopted. If an axial ligand is present, it is only weakly associated with the inner coordination sphere. The geometrical and electronic considerations for square-pyramidal geometries are very similar to those of the octahedral case because removal of the apical ligand trans to the oxo unit

does little to affect the overall splitting pattern of the parent pseudooctahedral energy level diagram; the MO of $d_{z^2}$ parentage is stabilized slightly from the octahedral case.

The oxo of a $d^2$ metal—oxo, and to a lesser extent a $d^4$ metal—oxo, is electrophilic and susceptible to nucleophilic attack. For example, salen-supported metal—oxos react as epoxidation catalysts, where the oxo moiety is transferred to nucleophilic olefin.[51,52] The nucleophilic attack of an olefin on $Mn^V(O)$ is intriguing because this reaction is exemplary of the AB strategy of Chart 1 (AB). O—O bond formation follows by replacement of the two-electron bond of the olefin by the lone pair of hydroxide. Although simple in construct, the reaction is difficult to effect because the $OH^-$ nucleophile is thermodynamically considerably more difficult to oxidize than the double bond of an olefin. In addition, unlike olefins, the oxidation of hydroxide also demands management of protons and hence relies on control of redox reactions coupled to the proton.[20,53–55]

We have addressed the challenges confronting the implementation of the AB strategy for O—O bond formation with the construction of Hangman porphyrins[56,57] and related macrocyclic platforms.[58,59] The Hangman construct replaces

(49) Wada, T.; Tsuge, K.; Tanaka, K. *Inorg. Chem.* **2001**, *40*, 329–337.

(50) Muckerman, J. T.; Polyansky, D. E.; Wada, T.; Tanaka, K.; Fujita, E. *Inorg. Chem.* **2008**, in this issue.

(51) *Comprehensive Asymmetric Catalysis*; Jacobsen, E. N., Pfaltz, A., Yamamoto, H., Eds.; Springer: New York, 1999; Vols. *I–III*.

(52) Jacobsen, E. N. *Acc. Chem. Res.* **2000**, *33*, 421–431.

(53) Rosenthal, J.; Bachman, J.; Dempsey, J. L.; Esswein, A. E.; Gray, T. G.; Hodgkiss, J. M.; Manke, D. R.; Luckett, T. D.; Pistorio, B. J.; Veige, A. S.; Nocera, D. G. *Coord. Chem. Rev.* **2005**, *249*, 1316–1326.
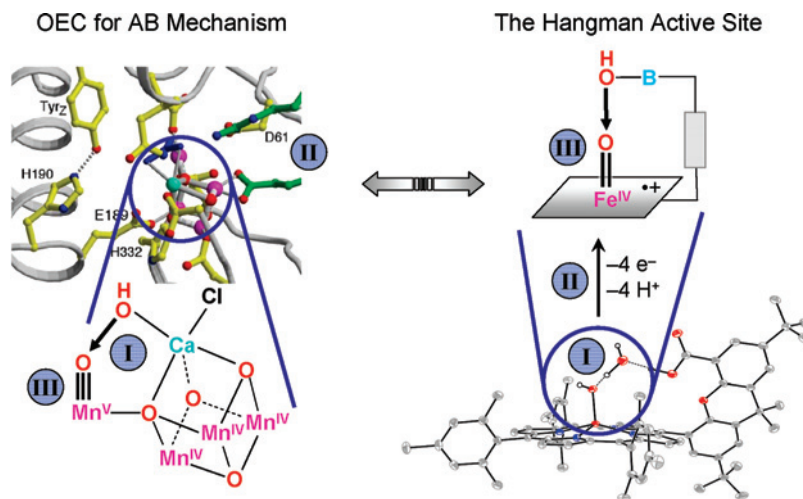
(54) Dempsey, J. L.; Esswein, A. E.; Manke, D. R.; Rosenthal, J.; Soper, J. D.; Nocera, D. G. *Inorg. Chem.* **2005**, *44*, 6879–6892.

(55) Reece, S. Y.; Hodgkiss, J. M.; Stubbe, J.; Nocera, D. G. *Philos. Trans. R. Soc. London, Ser. B* **2006**, *361*, 1351–1364.

(56) Yeh, C.-Y.; Chang, C. J.; Nocera, D. G. *J. Am. Chem. Soc.* **2001**, *123*, 1513–1514.

(57) Chng, L. L.; Chang, C. J.; Nocera, D. G. *Org. Lett.* **2003**, *5*, 2421–2424.

(58) Liu, S.-Y.; Nocera, D. G. *J. Am. Chem. Soc.* **2005**, *127*, 5278–5279.

**Figure 6.** Water oxidation center in photosystem II[9] and the Hangman porphyrin[60] that (I) assemble the oxygens of two waters for coupling, (II) activate the water to oxo by proton-coupled electron transfer, and (III) position a high-valent oxo along the reactive metal hydroxide vector. Though the resting state of the Hangman is a $Fe^{III}-OH\cdots H_2O$ complex, the Hangman porphyrin is prepared by the introduction of $Fe^{II}$ into the porphyrin core and the assembly of two waters. Production of the Cpd I intermediate of the Hangman thus results from an overall $(4e^-,4H^+)$ process.

one porphyrin redox subunit of the Pacman architecture with an AB functionality. The precise positioning of the "hanging" group above the porphyrin macrocycle provides a scaffold to suspend an exogenous water molecule, with a moderate binding energy,[60] over another that is coordinated to the $Fe^{III}$ center of a heme platform. The electrophilic $d^4$ iron−oxo of Cpd I has been observed for the Hangman heme by cryogenic stopped-flow spectroscopy.[61]

The connection of the Hangman active site to the proposed $\{Mn^{IV}_3Mn^V\}$ $S_4$ state of OEC is highlighted in Figure 6. Both centers assemble two water molecules within a cleft. An electrophilic oxo in a tetragonal ligand is produced at either center by proton-coupled electron-transfer redox reactions.[62–72] For the case of the proposed model for the $S_4$ state of OEC, the oxo is bonded to a $d^2$ center of $Mn^V$, whereas for the Hangman cofactor, the oxo is bonded to a $d^4$ metal center of $Fe^{IV}$. Both OEC and the Hangman porphyrins

possess a proximate site to deliver hydroxide (from the $Ca^{2+}$ in OEC and from the hanging group in Hangman) to the oxo, which is susceptible to nucleophilic attack. As with heme peroxidases, the electrophilic oxo, $P^{\bullet+}Fe^{IV}=O$, is susceptible to attack by nucleophiles such as two electrons of the $\pi$ bond of olefins.[60,73] However, in the case of the Hangman cofactor, nucleophile attack by hydroxide remains to be demonstrated. The goal now is to see if the oxo is sufficiently electrophilic to be attacked by hydroxide. If not, the porphyrin can be modified with electron-withdrawing groups such as pentafluorinated phenyls in the meso positions[45] with the aim of increasing the electrophilicity of the $P^{\bullet+}Fe^{IV}=O$.

## 5. Metal−Oxo Cofactors in Trigonal Ligand Fields

**5.1. Trigonal-Bipyramidal Metal−Oxo Complexes.** The lowest-lying metal-based orbitals in the trigonal-bipyramidal geometry shown in Figure 3B comprise a degenerate e set (approximately $d_{xz}$ and $d_{yz}$), which limits stabilization of a metal−oxo triple bond to metals with a $d^0$ configuration. A slightly reduced bond order can be accommodated with a $d^1$ metal, but higher d electron counts are not likely tolerated for metal−oxos in this ligand field. In support of this contention, group V metal−oxos with the metal in a formal oxidation state of 4+ or 5+ are known to accommodate a terminal oxo complex in this geometry, but any metal from groups VI or higher leads to destabilization of the oxo linkage upon population of the M−O $\pi^*$ orbitals and examples of

(59) Yang, J. Y.; Bachmann, J.; Nocera, D. G. *J. Org. Chem.* **2006**, *71*, 8706–8714.

(60) Chang, C. J.; Chng, L. L.; Nocera, D. G. *J. Am. Chem. Soc.* **2003**, *125*, 2866–2876.

(61) Soper, J. D.; Kryatov, S. V.; Rybak-Akimova, E. V.; Nocera, D. G. *J. Am. Chem. Soc.* **2007**, *129*, 5069–5075.

(62) Cukier, R. I.; Nocera, D. G. *Annu. Rev. Phys. Chem.* **1998**, *49*, 337–369.

(63) Rosenthal, J.; Young, E. R.; Nocera, D. G. *Inorg. Chem.* **2007**, *46*, 8668–8675.

(64) Rosenthal, J.; Hodgkiss, J. M.; Young, E. R.; Nocera, D. G. *J. Am. Chem. Soc.* **2006**, *128*, 10474–10483.

(65) Hodgkiss, J. M.; Damrauer, N. H.; Pressé, S.; Rosenthal, J.; Nocera, D. G. *J. Phys. Chem. A* **2006**, *110*, 18853–18858.

(66) Damrauer, N. H.; Hodgkiss, J. M.; Rosenthal, J.; Nocera, D. G. *J. Phys. Chem. B* **2004**, *108*, 6315–6321.

(67) Stubbe, J.; Nocera, D. G.; Yee, C. S.; Chang, M. C. Y. *Chem. Rev.* **2003**, *103*, 2167–2202.

(68) Roberts, J. A.; Kirby, J. P.; Wall, S. T.; Nocera, D. G. *Inorg. Chim. Acta* **1997**, *263*, 395–405.

(69) Deng, Y.; Roberts, J. A.; Peng, S.-M.; Chang, C. K.; Nocera, D. G. *Angew. Chem., Int. Ed.* **1997**, *36*, 2124–2127.

(70) Kirby, J. P.; Roberts, J. A.; Nocera, D. G. *J. Am. Chem. Soc.* **1997**, *119*, 9230–9236.

(71) Roberts, J. A.; Kirby, J. P.; Nocera, D. G. *J. Am. Chem. Soc.* **1995**, *117*, 8051–8052.

(72) Turró, C.; Chang, C. K.; Leroi, G. E.; Cukier, R. I.; Nocera, D. G. *J. Am. Chem. Soc.* **1992**, *114*, 4013–4015.

(73) Yang, J. Y.; Nocera, D. G. *J. Am. Chem. Soc.* **2007**, *129*, 8192–8198.

(74) MacBeth, C. E.; Golombek, A. P.; Young, V. G., Jr.; Yang, C.; Kuczera, K.; Hendrich, M. P.; Borovik, A. S. *Science* **2000**, *289*, 938–941.

(75) MacBeth, C. E.; Gupta, R.; Mitchell-Koch, K. R.; Young, V. G., Jr.; Lushington, G. H.; Thompson, W. H.; Hendrich, M. P.; Borovik, A. S. *J. Am. Chem. Soc.* **2004**, *126*, 2556–2567.

(76) Budria, J. G.; Raugei, S.; Cavallo, L. *Inorg. Chem.* **2006**, *45*, 1732–1738.

(77) Hu, X.; Meyer, K. *J. Am. Chem. Soc.* **2004**, *126*, 16322–16323.

(78) Shi, Y.; Cao, C.; Odom, A. L. *Inorg. Chem.* **2004**, *43*, 275–281.
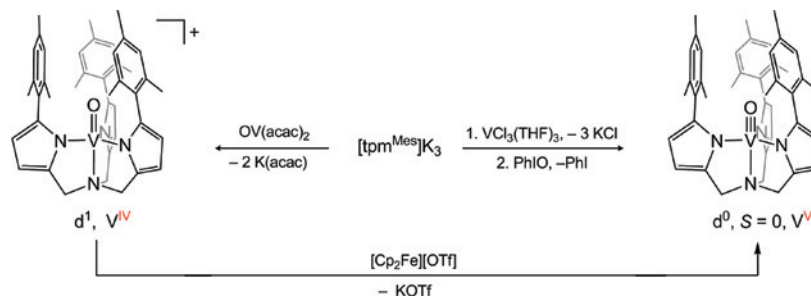
**Figure 7.** Tris(pyrrolide)amine framework with attendant details for a metal−oxo chemistry involving vanadium. See the Experimental Methods for details of preparation.

such oxos are more unusual. For instance, consider the tris(urea)amine scaffold developed by Borovik and co-workers:[74]



(1)
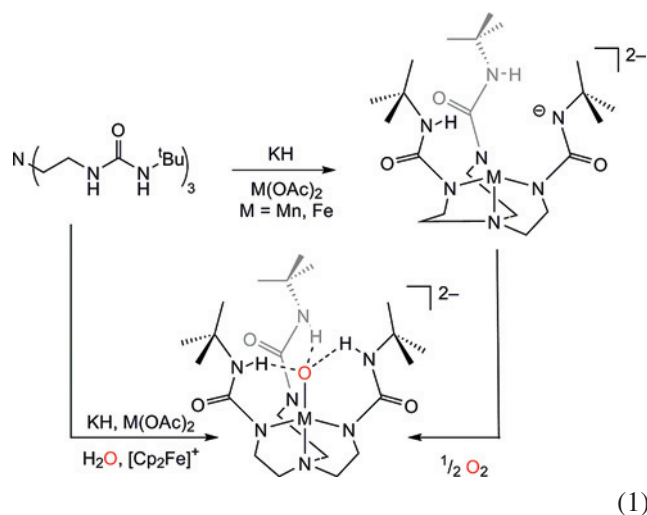
Two key observations related to the water oxidation problem have been made with this system: (1) oxygen bond homolysis between two metal ions is observed to produce two terminal metal oxide complexes (the microscopic reverse of an O−O bond-making event);[74] (2) through control of the secondary bonding environment, the conversion of a water molecule into a terminal oxide species has been observed.[75] Recent computations indicate that the oxygen cleavage reaction may indeed proceed through a terminal oxo intermediate of a M−O bond order exceeding 1 (where the apical nitrogen is not bound);[76] however, this terminal oxo, if it exists, has only a fleeting existence on its way to the singly bonded iron oxide product. In the final product, the singly bonded oxide is accompanied by extensive hydrogen bonding to the three pendant urea N−H bonds in the ligand's secondary coordination. We note that nitrene capture by a tris(carbene-α-methyl)amine-supported Co$^I$ center results in a four-coordinate imido species where the apical nitrogen is unbound,[77] thus providing a snapshot of an isoelectronic intermediate of the transient oxo complex.

We have explored new ligand scaffolds that systematically allow us to examine the trigonal-bipyramidal geometry for terminal metal−oxos. The tris(pyrrolyl-α-methyl)amine framework shown in Figure 7 is a variant of Odom's development of a parent tris(pyrrolyl) ligand scaffold.[78] Substitution of

2-mesitylpyrrole[79] for pyrrole in Odom's reported synthesis of tris(pyrrolyl-α-methyl)amine produces the target tris(pyrrolyl-α-methyl-δ-mesityl)amine ligand in high yields. A family of vanadium complexes utilizing this ligand framework have been synthesized, utilizing the (tpa$^{Mes}$)V$^{III}$(THF) synthon as a convenient precursor to various V$^{IV}$ species and V$^V$ oxo complexes [tpa$^{Mes}$ = tris(pyrrolyl-α-methyl-δ-mesityl)amine]. In a similar system, the trigonally coordinated V(Mes)$_3$ readily dimerizes with single O-atom bridges to form V$^{IV}$ species [(Mes)$_3$V$^{IV}$]$_2$($\mu$-O) (Mes = mesityl).[80] The large aryl substituents on the pyrrolyls circumvent this complication of dimer formation, thus allowing us to target terminal oxo complexes of V$^{IV}$. Our inclination is that the d$^0$ terminal metal−oxo will be too stable for O−O bond formation via an AB strategy. Thus, we have turned our attention toward a d$^1$ terminal metal−oxo with the objective of exploring the RC strategy of Chart 1. Reaction of the triply deprotonated (tpa$^{Mes}$) ligand with a suitable vanadyl precursor [e.g., OV(acac)$_2$, OVOSO$_3$·$x$H$_2$O] provides access to the targeted terminal V$^{IV}$−oxo complexes as outlined in Figure 7. Current efforts are directed toward assessing the critical issue with regard to a RC strategy as to the extent to which radical character resides on the oxo versus the metal center in terminal oxos residing in a trigonal-bipyramidal ligand field.

Whereas radical character at the oxygen of the (M−O)$_{tbp}$ center is critical to advancing the RC strategy for O−O bond coupling, this criterion alone is insufficient. A RC strategy demands that *two* oxos residing in the trigonal-bipyramidal scaffold be convergent for their coupling. We have responded to this challenge with the synthesis of the cryptands shown in Figure 8. The active site combines the features of the metal binding sites of tris(2-aminoethyl)amine[81] and the neutral hexacarboxamide cryptand.[82] A melding of these two distinct coordinations results in the first cryptates involving a hexaanionic ligand scaffold. The high negative charge of the ligand allows for the stabilization of two high-valent metal centers in a cofacial trigonal-bipyramidal geometry.
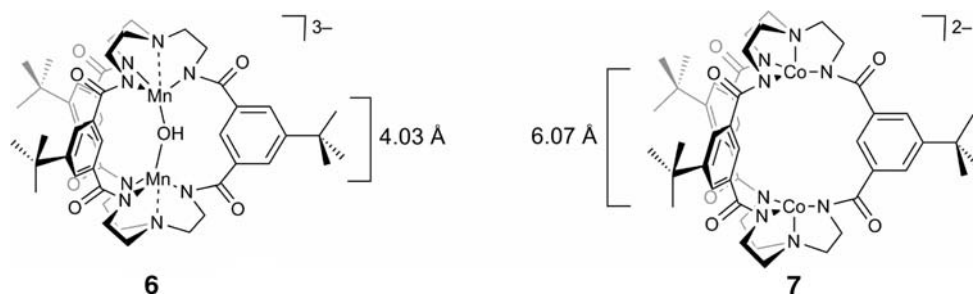
Manganese and cobalt have been introduced into the cavity; the resulting molecules shown in Figure 8 have been

(79) Rieth, R. D.; Mankad, N. P.; Calimano, E.; Sadighi, J. P. *Org. Lett.* **2004**, *6*, 3981–3983.

(80) Odom, A. L.; Cummins, C. C. *J. Am. Chem. Soc.* **1995**, *117*, 6613–6614.

(81) Schrock, R. R. *Acc. Chem. Res.* **1997**, *30*, 9–16.

(82) Kang, S. O.; Llinares, J. M.; Powell, D.; Vander Velde, D.; Bowman-James, K. *J. Am. Chem. Soc.* **2003**, *125*, 10152–10153.

**Figure 8.** Hexaanionic cryptates to support the coupling of two high-valent oxos by a RC strategy.

structurally characterized.[83] A comparison of the two structures shed light on the nature of the cavity created by the hexacarboxamido ligand. Manganese complex **6** possesses a hydroxide ligand that imposes a Mn−Mn distance of 4.058 Å. With the absence of a bridging ligand, the metals relax to a Co−Co distance of 6.073 Å in **7**. The flex in the cavity results from rotation about the metal−amide bond, which allows the ligand to bring the metal centers together in an accordion-like motion. The new ligand thus has several attributes pertaining to a RC strategy. It (i) presents binding sites that can accommodate high-valent metal centers, a necessity for a trigonal-bipyramidal ligand geometry, (ii) permits the assembly of two metal−oxos within the cavity in a convergent orientation, and (iii) possesses a cavity able to flex over 2 Å, thus allowing oxos to be brought together for their subsequent radical coupling. Moreover, the utilization of carboxamide linkers should render these ligands resistant to oxidation, thus avoiding ligand degradation by reactive oxygen intermediates. Current efforts are focused at generating high-valent oxos within the cavity of the new ligand.

**5.2. Pseudotetrahedral Metal Complexes.** The removal of the axial ligand from a (M−O)$_{tbp}$ coordination sphere and pyramidalization of the equatorial ligands has the benefit of delivering the ligand field shown in Figure 3C. The distinguishing trait of this ligand field is that a degenerate e($d_{x^2−y^2}$,$d_{xy}$) level is lowest in energy and may accommodate up to four electrons in the case of a low-spin configuration without weakening the primary metal−oxo interaction. A $d^4(S = 2)$ or $d^6(S = 0)$ metal ion yields an electronic structure akin to the iron−oxo discussed in section 4.2. Hence, O−O bond formation may be driven at late transition metals of even electron counts (e.g., $d^4$ and possibly $d^6$) by nucleophilic attack of hydroxide or by radical coupling of two oxos for odd electron counts (e.g., $d^5$). Thus, targeting pseudotetrahedral frameworks allows, in principle, the AB and RC strategies to be probed with high-valent, middle-to-late transition metal ions that are both amenable to high oxidation states and tolerant of electron counts up to to four and five (and for the case of second- and third-row metals, possibly up to six electrons) without destabilizing the M−O linkage.

Late-transition-metal terminal oxo complexes to the right of the manganese triad on the periodic table are known. The first was reported by Wilkinson with his preparation of

(Mes)$_3$Ir$^V$(O).[84] Mechanistic studies suggest that a single Ir$^{III}$ center binds one molecule of oxygen, most likely in a side-bound fashion.[85] Formation of the oxygen adduct precedes the rate-limiting step, where a second Ir$^{III}$ ion attacks the Ir($\eta^2$-O$_2$) adduct, ultimately leading to O−O bond homolysis to yield the terminal oxo, which is the microscopic reverse



(2)
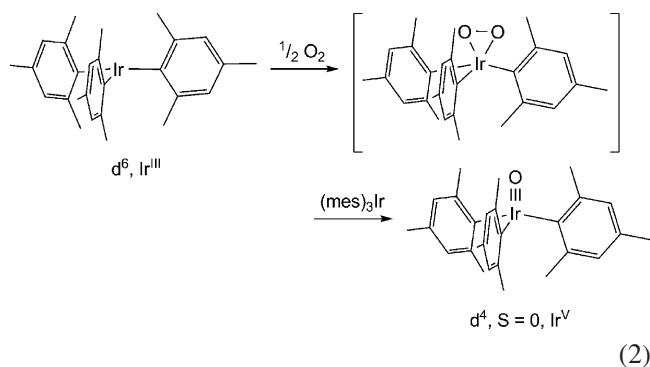
of the targeted O−O bond forming reactions. In a similar sequence of reactions, the monovalent, tris(pyrazolyl)borate cobalt complex, [Tp$^{Me,tBu}$]Co$^I$(N$_2$) ([Tp$^{Me,tBu}$] = hydridotris(3-*tert*-butyl-5-methylpyrazolyl)borate), reacts with oxygen to form a Co$^{II}$−superoxo species, which reacts with a second 1 equiv of Co$^I$. O−O bond homolysis is proposed to produce a transient Co−terminal oxo, which abstracts a H atom to produce the terminal hydroxo complex [Tp$^{Me,tBu}$]Co$^{II}$(OH):[86]

The disparate reaction paths for the first- and third-row late-transition-metal oxos follow directly from the MO diagram of Figure 3C. The resultant (mesityl)$_3$Ir$^V$(O) product has a $d^4$ electron configuration [approximately $(d_{x^2−y^2})^2(d_{xy})^2$], which is stable. Conversely, the intermediate cobalt−oxo [Tp$^{Me,tBu}$]Co$^{III}$(O) has a $d^6$ configuration [$(d_{xy})^2$-$(d_{x^2−y^2})^2(d_{xz})^1(d_{yz})^1$ for $S = 1$], leaving at most a double bond between Co−O. The presence of the metalloradical character along the Co−O bond is evident from the observed hydrogen abstraction reactivity.

The generalization of the pseudooctahedral electronic structure for late-transition-metal oxos presents a ligand design challenge. The bite angle must be sufficiently

(83) Alliger, G. E.; Breiner, B.; Fu, R.; Cummins, C. C.; Nocera, D. G., manuscript in preparation.

(84) Hay-Motherwell, R. S.; Wilkinson, G.; Hussain-Bates, B.; Hursthouse, M. B. *Polyhedron* **1993**, *12*, 2009–2012.

(85) Jacobi, B. G.; Laitar, D. S.; Pu, L.; Wargocki, M. F.; DiPasquale, A. G.; Fortner, K. C.; Schuck, S. M.; Brown, S. N. *Inorg. Chem.* **2002**, *41*, 4815–4823.

(86) Egan, J. W., Jr.; Haggerty, B. S.; Rheingold, A. L.; Sendlinger, S. C.; Theopold, K. H. *J. Am. Chem. Soc.* **1990**, *112*, 2445–2446.

$$d^7, S = {}^3/_2, Co^{II}$$

(3)
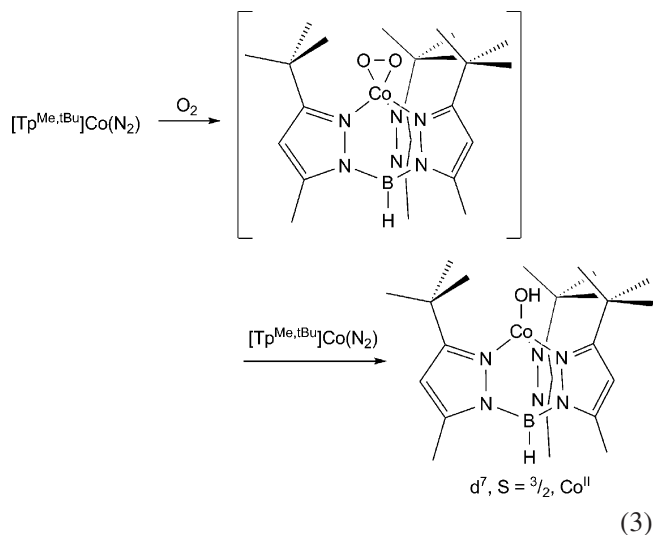
constricted to drive the $e(d_{xz},d_{yz})$ and $a(d_{z^2})$ levels to energies above $e(d_{x^2-y^2},d_{xy})$.[26] In addition, a structurally robust ligand scaffold is needed to fulfill other criteria including the following: (1) the $C_3$-symmetric ligand should be trianionic to achieve the desired middle-to-high oxidation states for the metal–oxo complexes; (2) the scaffold should be modular such that the steric protection about the oxo moiety can be tempered for isolation or promotion of bimolecular radical-coupling reactions; (3) the scaffold should be oxidatively robust such that the redox events are localized within the metal–oxo framework without deleterious ligand oxidation events; and (4) the scaffold should not be protolytically sensitive because the desired reaction medium involves water as a substrate.

Figure 9 illustrates a palette of tridentate scaffolds that have been designed in our laboratories and that meet the foregoing ligand design criteria.[87] They all derive from the versatile triamine precursor [**8**; tame = 1,1,1-tris(aminomethyl)ethane],[88] which is derived from a triazide. As a note of caution, the triazide may be handled safely as long as it is kept wet. Typically, we immediately convert the triazide to the amine so that the azide has a short residency time in our laboratories. The triamine synthon has been functionalized as depicted in Figure 9. The tris(*tert*-butylurea)ethane (**9**) ligand platform derived from the addition of *tert*-butylisocyanate to **8** is evocative of platforms synthesized by Borovik,[74,75] wherein the urea N–H functionalities allow us to control the secondary coordination sphere of the metal–oxo. Electronically, derivatizing the primary amines into urea functional groups also attenuates the $\pi$ basicity of the amines, making the platform more amenable to middle-to-late-transition-metal ions for which traditional primary or secondary amine ligands are typically too reducing.[89] Additionally, the incorporation of $\beta$ heteroatoms into the ligand framework presents possible labile ligand donors that may

serve to stabilize coordinatively unsaturated metal ion species. In this vein, the tris(alkylamide) (**10**) and tris(arylamide) (**11**) ligands were prepared via reaction of **8** with the appropriate acid chloride precursor and potassium hydroxide. Reaction of **8** with 2-chloro-4,6-dimethylpyrimidine provides access to the tris(pyrimidinylamine) ligand **12**. Here the N-donor $\pi$ electrons are delocalized into the aromatic pyrimidine unit. Reaction of **8** with triflic anhydride or chlorophosphates in the presence of base yields the tris(trifluorosulfonylamide)[90] and tris(phosphorylamide) ligands, **13** and **14**, respectively. The previously reported ligand **13** was particularly attractive because the highly electron-withdrawing trifluorosulfonyl moieties make the N–H proton very acidic.[90] The utilization of diarylphosphate moieties introduces steric protection into the metal coordination sphere while still attenuating the N-donor basicity.

With this library of ligand platforms in hand, investigations of the transition metal–oxo chemistry engendered by this ligand field are underway with emphasis on $d^4$ metals such as $Fe^{IV}$. Initial studies indicate that we can successfully metalate the triamide pocket using 3 equiv of base (e.g., KH) followed by reaction with a suitable divalent metal precursor (e.g., $FeBr_2$) in polar solvents. As a general synthetic route, we are subjecting the $Fe^{II}$ synthons to various chemical oxidants and O-atom-transfer reagents. The basic coordination chemistry of these ligands on iron and other metals in the transition series is actively being explored in our laboratories.

## 6. Future Prospects

The supply of secure, clean, sustainable energy is arguably the most important scientific and technical challenge facing humanity in the 21st century.[91–94] The imperative for the discipline of chemistry is to meet this energy need in a sustainable and environmentally responsible way. Water provides a source of hydrogen that severs the link to carbon-based fuel supplies. Nonetheless, a significant fundamental issue confronts hydrogen generation from water by metal catalysts. In driving any closed hydrogen photogeneration cycle, the oxidative half of the reaction must also be realized.[95] If water is the hydrogen source, then oxygen generation must be performed with similar efficacy as hydrogen generation. The challenge confronting water-splitting catalysis is immediately apparent when the reaction is parsed into the constituent redox half-reactions. The reductive generation of hydrogen from water splitting is a two-electron event involving two protons, whereas the oxidative generation of oxygen from water splitting requires four electrons and four protons. It is here that efficiencies

(87) Betley, T. A.; Surendranath, Y.; Childress, M. V.; Alliger, G. E.; Fu, R.; Cummins, C. C.; Nocera, D. G. *Philos. Trans. R. Soc. London, Ser. B* **2007**, DOI: 10.1098/rstb.2007.2226.

(88) Fleischer, E. B.; Gebala, A. E.; Levey, A.; Tasker, P. A. *J. Org. Chem.* **1971**, *36*, 3042–3044.

(89) Fulton, J. R.; Holland, A. W.; Fox, D. J.; Bergman, R. G. *Acc. Chem. Res.* **2002**, *35*, 44–56.

(90) Kanai, M.; Kuramochi, A.; Shibasaki, M. *Synthesis* **2002**, *14*, 1956–1958.

(91) Lewis, N. S.; Nocera, D. G. *Proc. Natl. Acad. Sci. U.S.A.* **2006**, *103*, 15729–15735.

(92) Nocera, D. G. *Dædulus* **2006**, *135*, 112–115.

(93) Eisenberg, R.; Nocera, D. G. *Inorg. Chem.* **2005**, *44*, 6799.

(94) Hoffert, M. I.; Caldeira, K.; Jain, A. K.; Haites, E. F.; Harvey, L. D. D.; Potter, S. D.; Schlesinger, M. E.; Schneider, S. H.; Watts, R. G.; Wigley, T. M. L.; Wuebbles, D. J. *Nature* **1998**, *395*, 881–884.

(95) Esswein, A. J.; Nocera, D. G. *Chem. Rev.* **2007**, *107*, 4022–4047.
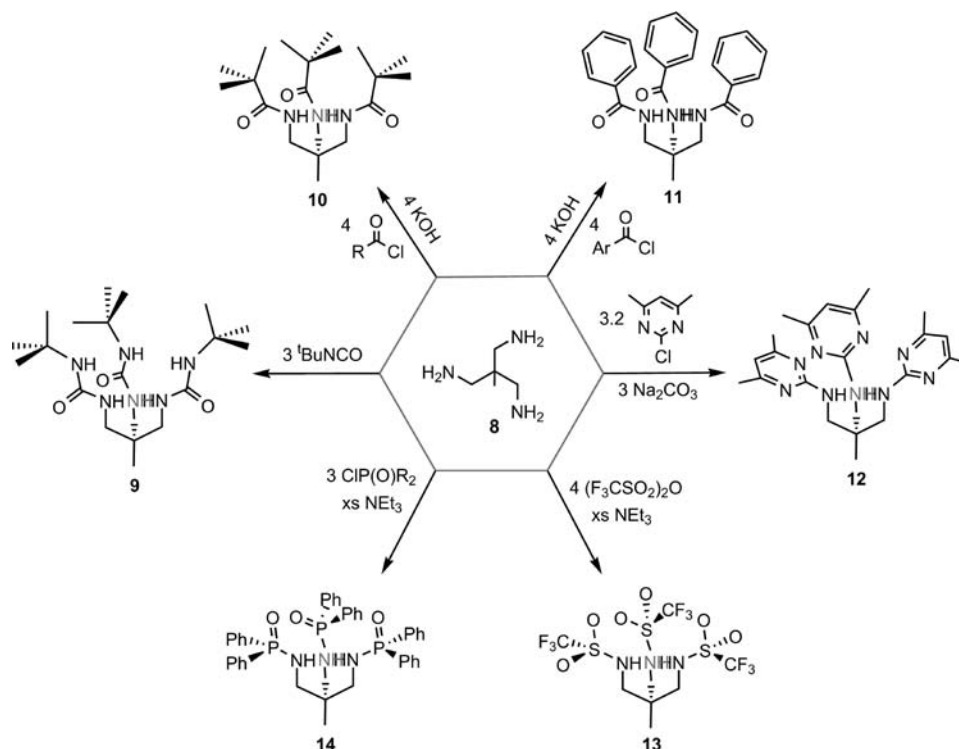
**Figure 9.** Trianionic, tridentate ligands to enforce the electronic structure in panel C of Figure 3 so that the synthesis of high oxidation state, terminal oxo formation on middle-to-late-transition-metal ions may be explored.

**Table 1.** M—O Coordination Environment and d Electron Count as It Pertains to O—O Bond Formation by AB or RC Strategies

| M—O coordination environment | O—O bond-forming reaction[a] | |
|---|---|---|
| | AB | RC |
| pseudo-$O_h$ | $d^0(3)$, $d^2(3)$, $d^4(2)$ | $d^1(3)$, $d^3(2.5)$ |
| tetragonal | $d^0(3)$, $d^2(3)$, $d^4(2)$ | $d^1(3)$, $d^3(2.5)$ |
| trigonal bipyramidal | $d^0(3)$ | $d^1(2.5)$ |
| pseudo-$T_d$ | $d^0(3)$, $d^2(3)$, $d^4(S = 2, 2)$ | $d^1(3)$, $d^3(2.5)$ |
| | $d^4(S = 0, 3)$, $d^6(S = 0, 2)$ | |

[a] Metal—oxo bond order is given in parentheses next to the d electron count.

suffer in the water-splitting reaction. New metal catalysts are needed that can effect the thermodynamically challenging reaction of a proton-coupled $(4e^-, 4H^+)$ transformation of two water molecules to oxygen.

The activation of the metal—oxo bond may proceed by two basic reaction types: acid–base or radical coupling. We present here various electronic structures of terminal metal—oxos that promote M—O bond activation and O—O bond formation, the fundamental step needed for oxygen generation. The various ligand fields that support AB or RC strategies are summarized in Table 1. In constructing Table 1, we note that only terminal metal—oxos, bound by a multiple bond to a single metal center, are considered. Alternatively, oxos may engage in single bonding to multiple metal centers. This motif is common in biology when oxygen is managed at cofactors composed of later metals such as copper.[96,97] An advantage of this approach is that the oxidizing equivalents are distributed among several metal

centers. Hence, the metal—oxo bond order is intrinsically lower than that of a single metal bound by a terminal oxo, and therefore the metal—oxo within a polynuclear core, especially one composed of late transition metals, will be more kinetically labile. However, the construction of the catalyst active site is more complicated inasmuch as multiple metals are involved. In the case of a single metal center, the proper ligand design allows the metal—oxo interaction to be isolated and controlled with fidelity. Hence, a reaction course for metal—oxo activation may be charted with greater predictability.

An often cited drawback of molecular catalysts is their instability. However, we point to the multitude of enzymes in biology that manage oxygen in harshly oxidizing environments. In all cases, the catalytic site is molecular and not a solid. For these systems, repair mechanisms are present to circumvent catalyst degradation. Similarly, advances in catalyst design for water splitting should consider strategies for self-healing and repair. This field of catalysis will be a major subject of study in itself. Along these lines, the common ligand architectures present today are not compatible with water oxidation. The organometallic chemistry of the past 40 years has driven the design of a vast library of ligands for reactions involving the bonds of carbon, nitrogen, and hydrogen. The catalysis of these bonds is performed in environments that are *reducing*. Consequently, many of these ligand designs do not stand up well to the water-splitting problem. Along this line, it should come as no surprise that the preponderance of ligands for water-splitting catalysts to date involve polypyridines and porphyrins. Of any common ligand set, these are perhaps the most stable to metal—oxos. However, if the area of water-splitting catalysis is to move

(96) Mirica, L. M.; Ottenwaelder, X.; Stack, T. D. P. *Chem. Rev.* **2004**, *104*, 1013–1046.

(97) Solomon, E. I.; Sarangi, R.; Woertink, J. S.; Augustine, A. J.; Yoon, J.; Ghosh, S. *Acc. Chem. Res.* **2007**, *40*, 581–591.

forward and the stereoelectronic structure is to be tailored to the water-splitting problem, then ligand design will have to step beyond these common ligand architectures. A major challenge will be the creation of new classes of ligands and ligand components that thrive under oxidizing conditions. Collins pioneered the ground-up design of oxidatively robust ligand frameworks,[98–100] but there has been little follow-up on this original work. In general, oxidatively stable catalyst components need to be identified, understood, and efficiently incorporated into next-generation functional catalyst architectures.

We conclude by noting that an alternative approach to the molecular metal−oxos described includes the design of oxos in the solid state. The drawback here is that mechanistic insights, at a detailed level, are difficult to garner for oxides on surfaces. In almost all cases of heterogeneous catalysis, we know little about the site of catalysis and its composition, structure, and activity. We seldom know the mechanism by which the catalysis proceeds. A deeper fundamental understanding of the structure and function of the heterogeneous catalytic active site will allow us to create more active, selective, and robust catalysts. It is here that molecular water-splitting catalysis finds another imperative for its pursuit. Because the molecular metal oxos lend themselves better to mechanistic analysis, their study can provide a guidepost for the development of metal oxide water-splitting catalysts.

## 7. Experimental Methods

**General Considerations.** All manipulations were carried out in a nitrogen-filled glovebox or under an inert atmosphere provided by a Schlenk line unless otherwise noted. All solvents were reagent grade (Aldrich) or better and were dried and degassed by standard methods. *tert*-Butylisocyanate (Aldrich), pivaloyl chloride (Aldrich), benzoyl chloride (Aldrich), triflic anhydride (Aldrich), and chlorodiphenylphosphine oxide (Aldrich) were purchased from the commercial sources indicated and used as received. 1,1,1-Tris(aminomethyl)ethane·3HCl (tame·3HCl)[88] and 2-chloro-4,6-dimethylpyrimidine[101] were prepared by literature procedures.

**Methods.** NMR data were recorded at the MIT Department of Chemistry Instrument Facility (DCIF) on a Varian Mercury 300 spectrometer. NMR solvents (CD$_3$Cl, DMSO-$d_6$, and CD$_3$CN) were purchased from Cambridge Isotope Laboratory and purified by standard procedures prior to use.[102] $^1$H NMR (300 MHz) and $^{13}$C{$^1$H} (75 MHz) spectra were referenced to residual solvent peaks and recorded at room temperature unless otherwise noted. $^{31}$P{$^1$H} NMR (121.4 MHz) spectra were referenced to an external 85% H$_3$PO$_4$ standard and recorded at room temperature unless otherwise noted. All chemical shifts are reported in the standard $\delta$ notation in parts per million. Elemental analyses were performed by Desert Analytics, Tucson, AZ.

Electrochemistry was performed with a standard three-electrode configuration using a CV-50W potentiostat (Bioanalytical Systems). The working electrode was glassy carbon, the auxiliary electrode was a platinum wire, and the reference was a saturated calomel electrode. Electrochemical samples consisted of the complex dissolved in water at pH = 6.8 and containing 0.1 M KPF$_6$ as the supporting electrolyte.

**Preparation of MeC(CH$_2$NHCONH$^t$Bu)$_3$ (9).** Potassium hydroxide (5.66 g, 0.101 mol) was added to tame·3HCl (7.62 g, 0.034 mol) dissolved in 150 mL water at room temperature. The solution was stirred vigorously for 30 min. A solution of *tert*-butyl isocyanate (10 g, 0.101 mol) in 50 mL of THF was added portionwise to the aqueous solution. After stirring for 2 h at room temperature, the solution was extracted with a 1:1 Et$_2$O/THF solution (3 × 150 mL). The combined organic fractions were washed with a saturated brine solution and dried over MgSO$_4$, and then the solvent was removed via rotary evaporation to produce a white solid. The white solid was washed with pentane (200 mL) to form a finely divided powder, which was collected via filtration through a fritted funnel and then dried in vacuum (13.66 g, 98%). $^1$H NMR (DMSO-$d_6$) $\delta$/ppm: 5.861 (s, 3H, RCON*H*$^t$Bu), 5.727 (t, $J$ = 6 Hz, 3H, RN*H*CONH$^t$Bu), 2.716 (d, $J$ = 6 Hz, 6H, MeC(C*H*$_2$NHCONH$^t$Bu)$_3$), 1.207 (s, 27H, RC(C*H*$_3$)$_3$), 0.59 (s, 3H, (*H*$_3$C)CR$_3$). $^{13}$C{$^1$H} NMR (DMSO-$d_6$) $\delta$/ppm: 157.89, 49.01, 42.78, 40.5, 29.36, 18.41. Anal. Calcd for C$_{20}$H$_{42}$N$_6$O$_3$: C, 57.94; H, 10.21; N, 20.27. Found: C, 58.06; H, 10.33; N, 20.29.

**Preparation of MeC(CH$_2$NHCO$^t$Bu)$_3$ (10).** Potassium hydroxide (12.0 g, 0.214 mol) was dissolved in 20 mL water and added to a solution of tame·HCl (8.076 g, 0.036 mol) dissolved in a 50 mL solution of THF and water (1:1) at room temperature. The solution was stirred vigorously for 30 min and then cooled in an ice bath. Pivaloyl chloride (21.46 g, 0.178 mol) was added via pipet to the stirring solution at 0 °C. The reaction was allowed to warm to room temperature over several hours. The solution was extracted with a 1:1 Et$_2$O/THF solution (3 × 150 mL). The combined organic fractions were washed with a 0.1 M NaOH solution (200 mL) and a saturated brine solution (200 mL) dried over MgSO$_4$, and then the solvent was removed via rotary evaporation to produce a white solid. The white solid was washed with pentane (200 mL) to form a finely divided powder, which was collected via filtration through a fritted funnel and then dried in vacuum (11.99 g, 91%). $^1$H NMR (DMSO-$d_6$) $\delta$/ppm: 7.764 (t, $J$ = 6.6 Hz, 3H, RN*H*CO$^t$Bu), 2.787 (d, $J$ = 6.6 Hz, 6H, MeC(C*H*$_2$NHCO$^t$Bu)$_3$), 1.136 (s, 27H, RC(C*H*$_3$)$_3$), 0.63 (s, 3H, (*H*$_3$C)CR$_3$). $^{13}$C{$^1$H} NMR (DMSO-$d_6$) $\delta$/ppm: 164.81, 46.51, 42.82, 40.5, 28.29, 19.33. Anal. Calcd for C$_{20}$H$_{39}$N$_3$O$_3$: C, 65.00; H, 10.64; N, 11.37. Found: C, 65.36; H, 10.98; N, 11.05.

**Preparation of MeC(CH$_2$NHCOPh)$_3$ (11).** Potassium hydroxide (12 g, 0.214 mol) was dissolved in 20 mL of water and added to a solution of tame·3HCl (8.076 g, 0.036 mol) dissolved in a 50 mL solution of THF and water (1:1) at room temperature. The solution was stirred vigorously for 30 min and then cooled in an ice bath. Benzoyl chloride (25.02 g, 0.178 mol) was added via pipet to the stirring solution at 0 °C. The reaction was allowed to warm to room temperature over several hours. The solution was extracted with a 1:1 Et$_2$O/THF solution (3 × 150 mL). The combined organic fractions were washed with a 0.1 M NaOH solution (200 mL) and a saturated brine solution (200 mL) and dried over MgSO$_4$, and then the solvent was removed via rotary evaporation to produce a white solid. The white solid was washed with pentane (2 × 200 mL) to form a finely divided powder, which was collected via filtration through a fritted funnel and then dried in vacuum (14.24 g, 93%). $^1$H NMR (DMSO-$d_6$) $\delta$/ppm: 8.724 (t, $J$ = 6.3 Hz, 3H, RN*H*COPh), 7.920 (m, 6H, *o*-C$_6$*H*$_5$), 7.49–7.58 (m, 9H, *m*/*p*-C$_6$*H*$_5$), 3.263 (d, $J$ = 6.6 Hz, 6H, MeC(C*H*$_2$NHCOPh)$_3$), 0.896 (s, 3H, (*H*$_3$C)CR$_3$). $^{13}$C{$^1$H} NMR (DMSO-$d_6$) $\delta$/ppm: 167.21, 134.22,

(98) Collins, T. J. *Acc. Chem. Res.* **1994**, *27*, 279–285.

(99) Patterson, R. E.; Gordon-Wylie, S. W.; Woomer, C. G.; Norman, R. E.; Weintraub, S. T.; Horwitz, C. P.; Collins, T. J. *Inorg. Chem.* **1998**, *37*, 4748–4750.

(100) Horwitz, C. P.; Fooksman, D. R.; Vuocolo, L. D.; Gordon-Wylie, S. W.; Cox, N. J.; Collins, T. J. *J. Am. Chem. Soc.* **1998**, *120*, 4867–4868.

(101) Vlád, G.; Horváth, I. T. *J. Org. Chem.* **2002**, *67*, 6550–6552.

(102) Armarego, W. L. F.; Perrin, D. D. *Purification of Laboratory Chemicals*, 4th ed.; Butterworth-Heinemann: Oxford, U.K., 1996.

131.57, 128.61, 127.16, 43.34, 42.10, 19.58. Anal. Calcd for $C_{26}H_{27}N_3O_3$: C, 72.71; H, 6.34; N, 9.78. Found: C, 72.56; H, 6.69; N, 9.46.

**Preparation of MeC(CH₂NH(3,5-dimethylpyrimidine))₃ (12).** Tris(aminomethyl)ethane (tame) was prepared from tame·3HCl as reported in the literature and distilled as a means of purification.[103] 2-Chloro-4,6-dimethylpyrimidine (10.0 g, 0.070 mol) was dissolved in THF (25 mL) and added to a solution of tame (2.57 g, 0.022 mol) in THF (10 mL) and water (5 mL) at room temperature. Solid Na₂CO₃ (7.434 g, 0.070 mol) was added to the mixture, which was stirred vigorously at room temperature for 6 h. The solution was extracted with dichloromethane (3 × 75 mL). The combined organic fractions were washed with a 0.1 M NaOH solution (200 mL) and a saturated brine solution (200 mL) and dried over MgSO₄, and then the solvent was removed via rotary evaporation to produce a white solid. The white solid was washed with pentane (2 × 100 mL) to form a finely divided powder, which was collected via filtration through a fritted funnel and then dried in vacuum (7.92 g, 83%). ¹H NMR (DMSO-$d_6$) $\delta$/ppm: 7.824 (t, $J$ = 6.6 Hz, 3H, RN*H*), 6.303 (s, C_Ar−H), 3.170 (d, $J$ = 6.6 Hz, 6H, MeC-(C*H*₂NH(pyrm))₃), 2.18–2.27 (m, 18H, pyrm(C*H*₃)₂), 0.777 (s, 3H, (*H*₃C)CR₃). ¹³C{¹H} NMR (DMSO-$d_6$) $\delta$/ppm: 167, 162.75, 108.61, 44.06, 41.40, 23.47, 19.27. Anal. Calcd for $C_{23}H_{33}N_9$: C, 63.42; H, 7.64; N, 28.94. Found: C, 63.58; H, 7.79; N, 28.56.

**Preparation of MeC(CH₂NHSO₂CF₃)₃ (13).** This compound was prepared using a different protocol than that described in the literature.[90] The details of our synthesis are as follows: In an oven-dried, 250 mL, round-bottomed flask, tame (2.077 g, 0.018 mol) and triethylamine (7.17 g, 0.071 mol; anhydrous) were diluted with 100 mL of anhydrous dichloromethane. The flask was sparged with dinitrogen for 15 min, and then the reaction flask was cooled to −78 °C in a dry ice/acetone bath. Triflic anhydride (25 g, 0.089 mol) was introduced by syringe into the cold solution under a constant flow of dinitrogen. The solution was stirred vigorously and allowed to warm to room temperature over the course of 14 h. The solution was washed with a 2.5% NaHSO₄ solution (2 × 50 mL), and the aqueous layer was discarded. The material was extracted into a 0.1 M NaOH solution, and the organic layer was discarded. The basic solution was then acidified to a pH of 1 by the slow addition of 0.1 M HCl. The acidified solution was extracted into Et₂O (3 × 25 mL), and then the combined organic fractions were washed with a saturated brine solution (2 × 50 mL), dried with MgSO₄, and concentrated in vacuo. The resultant oil was triturated with pentane (2 × 25 mL) to form a finely divided powder, which was dried in vacuum (6.19 g, 68%). The product purity was confirmed by comparing the ¹H and ¹⁹F{¹H} spectra with the reported values.[90]

**Preparation of MeC(CH₂NHPOPh₂)₃ (14).** In an oven-dried, 250 mL, round-bottomed flask, tame (1.27 g, 0.011 mol) and anhydrous triethylamine (4.4 g, 0.043 mol) were diluted with 100 mL of anhydrous dichloromethane. The flask was sparged with dinitrogen for 15 min, and then the reaction flask was cooled to −78 °C in a dry ice/acetone bath. Chlorodiphenylphosphine oxide (9 g, 0.038 mol) was introduced by syringe into the cold solution under a constant flow of dinitrogen. The solution was stirred vigorously and allowed to warm to room temperature over the course of 10 h. The solution was washed with a 2.5% NaHSO₄ solution (2 × 50 mL), and the aqueous layer was discarded. The organic fraction was washed with a 0.1 M NaOH solution (200 mL) and a saturated brine solution (200 mL) and dried over MgSO₄, and then volatiles were removed via rotary evaporation to produce a white solid. The white solid was washed with pentane (2 × 100 mL) to form a finely divided powder, which was collected via filtration through a fritted funnel and then dried in vacuum (6.32 g, 81%). ¹H NMR (acetone-$d_6$) $\delta$/ppm: 7.85–7.91 (m, 10H, C_Ar−H), 7.76–7.81 (m, 2H C_Ar−H), 7.35–7.54 (m, 18H C_Ar−H), 5.923 (m, 3H, RCH₂N*H*P(O)Ph₂), 2.84 (m, 6H, MeC(C*H*₂NHP(O)Ph₂)₃), 0.834 (s, 3H, (*H*₃C)CR₃). ³¹P{¹H} NMR (acetone-$d_6$) $\delta$/ppm: 26. Anal. Calcd for $C_{41}H_{42}N_3O_3P_3$: C, 68.61; H, 5.90; N, 5.85. Found: C, 68.96; H, 6.12; N, 5.84.

Electronic structure calculations were performed with the *Q-Chem*[104] program package using the density functional theory method of B3LYP.[105–107] The LANL2DZ[108] effective core potential and basis set is used for ruthenium, and the 6-31G(*) basis set is used for all other elements. Constrained optimization is carried out by only fixing the O−O distance with all other degrees of freedom relaxed.

(103) Brown, K. N.; Hockless, D. C. R.; Sargeson, A. M. *J. Chem. Soc., Dalton Trans.* **1999**, 2171–2175.

(104) Shao, Y.; Molnar, L. F.; Jung, Y.; Kussmann, J.; Ochsenfeld, C.; Brown, S. T.; Gilbert, A. T. B.; Slipchenko, L. V.; Levchenko, S. V.; O'Neill, D. P. *Phys. Chem. Chem. Phys.* **2006**, *8*, 3172–3191.
(105) Becke, A. D. *J. Chem. Phys.* **1993**, *98*, 5648–5652.
(106) Becke, A. D. *Phys. Rev. A* **1988**, *38*, 3098–3100.
(107) Lee, C.; Yang, W.; Parr, R. G. *Phys. Rev. B* **1988**, *37*, 785–789.
(108) Hay, P. J.; Wadt, W. R. *J. Chem. Phys.* **1985**, *82*, 270–283.